Band structure of the odd-even ^{125}La, ^{127}La nuclei

K. Starosta, Ch. Droste, T. Morek, and J. Srebrny
Institute of Experimental Physics, Warsaw University, Hoża 69, 00-681 Warsaw, Poland

D. B. Fossan, D. R. LaFosse, H. Schnare, I. Thorslund, P. Vaska, and M. P. Waring
Department of Physics, State University of New York at Stony Brook, Stony Brook, New York 11794

W. Satuła and S. G. Rohoziński
Institute of Theoretical Physics, Warsaw University, Hoża 69, 00-681 Warsaw, Poland

R. Wyss
The Royal Institute of Technology, Physics Department, Frescati, Frescativägen 24, S-104 05 Stockholm, Sweden

I. M. Hibbert, R. Wadsworth, and K. Hauschild
Department of Physics, University of York, Heslington, York Y01 5DD, United Kingdom

C. W. Beausang, S. A. Forbes, P. J. Nolan, and E. S. Paul
Oliver Lodge Laboratory, University of Liverpool, P.O. Box 147, Liverpool L69 3BX, United Kingdom
(Received 29 September 1995)

Excited states of the ^{125}La and ^{127}La nuclei were populated following ^{112}Sn(^{16}O,$p2n$) and ^{112}Cd(^{19}F,$4n$) fusion-evaporation reactions, respectively, and investigated using methods of in-beam γ-ray spectroscopy. Five collective bands in ^{125}La, and eleven collective bands in ^{127}La were observed. The spin and/or parity assignments of excited states in these nuclei were based on angular-correlation and linear-polarization measurements. The experimental data are discussed and compared to the results of self-consistent total-Routhian-surface calculations including quadrupole pairing.

PACS number(s): 21.10.Re, 23.20.Lv, 27.60.+j, 21.60.Ev

I. INTRODUCTION

Neutron deficient nuclei from the mass $A\sim130$ region have been the subject of many experimental studies. The even-even nuclei from this region were one of the first examples of γ-soft nuclei [1]. Furthermore, odd-A La isotopes with $A=125$ to 137 were the first cases [2] where decoupled rotational bands were identified and interpreted in terms of a particle coupled to a triaxial even-even core [3]. Recent spectroscopic data also reveal many other phenomena of topical interest, such as shape coexistence, γ-vibrational bands, signature inversion, and band termination effects.

In the language of the deformed shell model, the variety of structures observed in the $A\sim130$ mass region can be associated with opposite shape driving forces due to valence protons and neutrons, respectively (see Ref. [4]). Valence protons, filling the lower part of the $h_{11/2}$ subshell, tend to stabilize nuclear shapes at prolate deformations, while the valence neutrons, being at or above the $h_{11/2}$ midshell, favor oblate or triaxial shapes. Such a situation leads to a shape coexistence phenomenon with the resulting equilibrium shapes as well as the shapes of local potential wells strongly depending on the underlying proton and neutron shell structure and pairing properties. Thus it is expected that the spectroscopy of these nuclei would provide rich data from which sensitive studies could be made of effective/residual nuclear interactions, adiabacity/diabacity of nuclear motion, rotation-vibration couplings, and formation of collectivity.

The present investigation of the ^{125}La and ^{127}La nuclei was triggered by the previous observation [5] of an unusually fast $15/2^-\rightarrow11/2^-E2$ transition in ^{127}La, implying enhanced collectivity, but followed by a drop in collectivity above the $15/2^-$ level. This research will be presented in two parts. In the current paper, the level schemes including the band structure of ^{125}La and ^{127}La will be presented; this includes γ-γ coincidence studies as well as angular-correlation and linear-polarization measurements. Eleven bands were observed in ^{127}La and five bands in ^{125}La. The detailed quasiparticle structure of these bands is interpreted by means of a self-consistent total Routhian surface (TRS) model. A second paper [6] will present the results of a detailed set of recoil distance (RDM) lifetime measurements in ^{125}La and ^{127}La. A collective core-quasiparticle coupling model [7] will be used to discuss the excitation energies and $E2$-$M1$ transition rates for low-spin states of both positive and negative parity bands.

Preliminary results [8] of the current work have been reported. An independent study of the ^{127}La level scheme by D. Ward *et al.* [9] has also been made. The two studies of ^{127}La are complementary in several respects; there is more information about high-spin levels in Ref. [9], while the current study includes γ-ray polarization measurements. Results from both studies of ^{127}La and the present results of ^{125}La are used in the theoretical interpretation.

II. EXPERIMENTAL PROCEDURE

A. γ-γ coincidence measurements

Excited states of ^{125}La were populated following the ^{112}Sn(^{16}O,$p2n$) reaction at a beam energy of 79 MeV. A 2.6 mg/cm^2 thick ^{112}Sn target, backed with ^{208}Pb to stop the recoil nuclei, was employed. The Stony Brook array consisting of 6 Compton-suppressed Ge detectors and a 14 element bismuth germanate (BGO) multiplicity filter was used to collect γ - γ coincidences. To reduce the intensity of the background radiation from β-decay and Coulomb excitation, data were recorded only when two or more BGO detectors fired.

The level scheme of ^{127}La was studied using the ^{112}Cd(^{19}F,$4n$) reaction at a beam energy of 85 MeV. A 3 mg/cm^2 thick ^{112}Cd target backed with ^{208}Pb was used. Data were collected using the TESSA-3 array, consisting of 16 Compton-suppressed Ge detectors and a 50-element BGO multiplicity/sum energy filter [10], which was located temporarily at Stony Brook.

The level schemes were constructed using coincidence relationships and relative intensities. In order to determine the multipolarity of the transitions, angular correlations of the γ rays were measured using the DCO (directional correlation of oriented states) method (see Ref. [11]). For both experiments, data from the detectors positioned perpendicular to the beam axis (at $\theta \approx 90°$) were sorted against data from the forward/backward detectors near the beam axis (at $\theta \approx 30°$, 150°) in an asymmetric DCO matrix. To extract the DCO ratios, gates were set on the well-known stretched $E2$ transitions on both axes.

B. Polarization measurements in ^{127}La

Taking into account the limitations of the DCO method regarding parity, linear polarizations of γ rays from ^{127}La were measured at Stony Brook utilizing a 5$\times$Ge Compton polarimeter with kinematic selection. The same target and reaction as in the γ-γ coincidence experiment were used. The γ-ray polarizations were measured in singles mode, which limited the method to the strongest γ lines in the spectrum. The central scattering detector of the polarimeter was positioned with its axis at $\theta = 90°$ with respect to the beam axis and 20 cm below the target. Four analyzing detectors were placed in a plane perpendicular to the central detector axis, at a distance of 7 cm, two of them perpendicular to the reaction plane (the reaction plane is defined by the beam axis and scattering detector) and two of them in the reaction plane. The Compton scattering events, i.e., coincidences between the central and one of the analyzing detectors, were recorded on magnetic tape. The γ-ray energy peaks were extracted by the summation of the energies deposited in the coincident scattering and analyzing detectors. Typical resolutions obtained from source tests were FWHM $\approx$3 keV for the 1408 keV ^{152}Eu γ ray. In order to enhance the peak/background ratio, events which did not fulfill the Compton kinematic scattering conditions for the polarimeter geometry were excluded in the event sorting (see Ref. [12]). Data were sorted into two spectra, one for the scatterer plus analyzers perpendicular to the reaction plane and the other for the scatterer plus analyzers in the reaction plane. The definition of the linear polarization used in this paper is

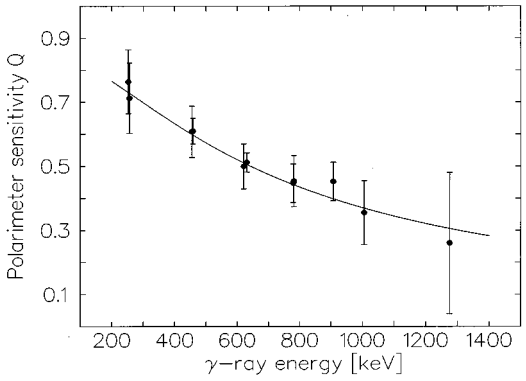

FIG. 1. 5$\times$Ge detector polarimeter sensitivity calibration.

$$P(\theta) = \frac{W(\theta,0°) - W(\theta,90°)}{W(\theta,0°) + W(\theta,90°)}, \tag{1}$$

where $W(\theta,\psi)$ is the yield of γ rays which are emitted at an angle θ relative to the beam axis and having a polarization vector in the plane at an angle ψ relative to the reaction plane. An experimental asymmetry (see Ref. [13]) is defined as

$$A(\theta = 90°, E_\gamma) = \frac{N_\perp(E_\gamma) - N_\parallel(E_\gamma)}{N_\perp(E_\gamma) + N_\parallel(E_\gamma)}, \tag{2}$$

where $N_\perp(E_\gamma)$ is the measured intensity of the γ line in the first spectrum, and $N_\parallel(E_\gamma)$ is the measured intensity of the γ line in the second spectrum. The asymmetry is related to the polarization defined above [Eq. (1)] by

$$P = \frac{1}{Q} \times A, \tag{3}$$

where Q is sensitivity of the polarimeter. The sensitivity of the polarimeter was calibrated using the strong transitions with known multipolarities observed in the experiment. The calibration sensitivity curve is presented in Fig. 1. It was found that the experimental sensitivity of the polarimeter Q normalized to the sensitivity of a polarimeter made of idealized point like detectors Q_0 is nearly energy independent and equals $Q/Q_0 = 0.85(10)$. This conclusion agrees with the calibration results for similar polarimeters (see Ref. [14]) and allowed interpolations of the calibration curve.

III. EXPERIMENTAL RESULTS

A. Spin/parity assignments for the ^{127}La excited states

The level scheme derived for the ^{127}La nucleus is presented in Fig. 2. In comparison to the earlier work [5], nine new collective structures have been extracted from the present data; the current experiment confirms the transition order in the yrast cascade (band 1) and side band 4. Intensity relations and cross-over transitions of the present experiment between bands 2 and 3 resulted however in changes in the order of transitions for the low energy part of band 2. The measured energies, DCO ratios, and polarizations as well as spin/parity assignments for the excited states in ^{127}La are summarized in Table I. Multipolarities of the γ rays were

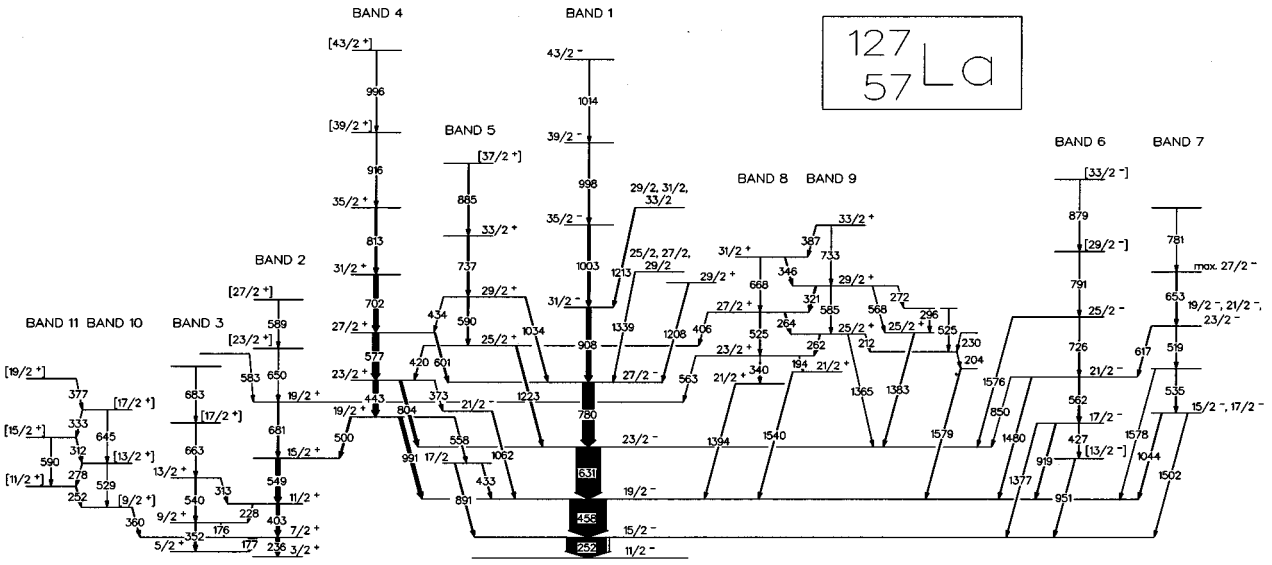

FIG. 2. ^{127}La level scheme.

determined by comparing the experimental DCO ratio and polarization values with those calculated for various possible spin/parity hypotheses [11]. The results of the DCO calculation for the 991-keV transition are displayed in Fig. 3, which is presented as a typical example. Figure 4 shows the polarization calculated [13] for different initial and final spin/parity possibilities for the 991-keV transition. The advantage of combining the DCO and polarization measurements can be seen from Fig. 3 and Fig. 4. The DCO function depends on the multipolarity but not on the electric or magnetic character of the transition. Conversely, the sign of the polarization depends on the type of the transition (see Fig. 4); for instance, with dipoles the polarization is negative for a pure stretched $M1$ and positive for a stretched $E1$ transition. In Fig. 5, experimental spectra from the polarization experiment are shown as an example. Although the DCO ratios for the 458-keV and 991-keV transitions are similar ($R_{\mathrm{DCO}}\approx 1$), but, as Fig. 5 shows, these two γ rays have opposite signs of the polarization. This method for spin/parity assignments is not able to distinguish between transitions with $\Delta I=+1$ and $\Delta I=-1$ (see Figs. 3 and 4). In cases of such ambiguity the solution in which spin increases with energy was chosen.

The level scheme obtained from the experimental data is similar to the results of the independent study of Ref. [9], although differences occur in spin assignments of several levels, which will be discussed. The spins of the yrast cascade (band 1) were known from the earlier study (see Refs. [5,2]). The DCO ratio for the 1208-, 1213-, and 1339-keV transitions suggest $|\Delta I|\leqslant 1$. The positive polarization measured for the 1208-keV γ ray suggests a stretched $E1$ character. In other cases, multipolarity assignments are ambiguous; the allowed spins in the current study are given in Fig. 2.

The spins assigned to band 4 are different from those proposed in Ref. [5] but are consistent with Ref. [9]. For the 991-keV transition, the R_{DCO} value and large negative polarization (see Fig. 5) exclude all the possibilities except $E1$ with $\Delta I=0$ or $M1+E2$ ($\delta\simeq\pm 1$) with $\Delta I=\pm 1$. The positive parity for the band 4 is proposed since the bandhead decays via stretched $E2$ transitions to the positive parity ground state (the positive parity is taken from the systematics—see discussion of the band 2). This gives the spin/parity of the lowest band member as $19/2^+$ rather than $21/2^+$ as proposed in Ref. [5]. The same arguments are valid for the 804-keV transition, although in this case only the sign of the polarization was determined. The 443-, 577-, 702-, and 813-keV intraband transitions have $R_{\mathrm{DCO}}\approx 1$ and polarization $P>0.2$ which are consistent with a stretched $E2$ character. Also, stretched $E2$ multipolarities are proposed for the 916- and 996-keV band transitions.

The multipolarities of the transitions placed below band 5 were determined from the DCO ratio only. For the 1062 keV transition, the R_{DCO} suggests mixed a $M1+E2$ character while the ratio for the 373-keV transition is consistent with a stretched $E1$, and so $21/2^-$ is proposed as the spin/parity for the intermediary level.

Band 5 is connected to the yrast structure by the 1034-keV and the 1223-keV transitions with R_{DCO} and polarization values consistent with stretched $E1$ transitions. The 420-keV and the 434-keV transitions connect band 5 with band 4; these γ rays have R_{DCO} values which suggest $M1+E2$ transitions with $|\Delta I|=1$. This determines the spin of the lowest member of the band to be $25/2^+$. The DCO ratios for the 590-keV and the 737-keV transitions are consistent with a stretched $E2$ character, and this assignment is also proposed for the 885-keV band transition.

Band 4 decays into band 2 via the 500-keV transition and then through the 549-, 403-, and 236-keV band-2 transitions to the bandhead. For all of these transitions, extracted $R_{\mathrm{DCO}}\approx 1$ ratios supported by positive polarizations suggest stretched $E2$ assignments, except for the 236-keV transition whose polarization was not determined. This implies that the bandhead spin is 3/2, with the positive parity taken from the odd-even La systematics ($3/2^+$ ground states are reported for ^{131}La [15], ^{129}La [16], and ^{123}La [17]). For the 681-, 650-, and 589-keV transitions of band 2, $R_{\mathrm{DCO}}\approx 1$. Based on

TABLE I. Observed γ-ray transitions and spin and/or parity assignments for excited states in ^{127}La.

Energy [a] [keV]	DCO ratio	Polarization	I_i^π	$\rightarrow$	I_f^π	Multipolarity	Band
175.9	0.7(3)		$9/2^+$	$\rightarrow$	$7/2^+$	$M1/E2$	3
176.6	0.86(6)		$7/2^+$	$\rightarrow$	$5/2^+$	$M1/E2$	2
194.2	0.36(6)		$23/2^+$	$\rightarrow$	$21/2^+$	$M1/E2$	8
204.0	0.7(1)					$M1/E2$	
212.0			$25/2^+$	$\rightarrow$			
227.6			$11/2^+$	$\rightarrow$	$9/2^+$	$M1/E2$ [d]	2
230.0							
236.0	0.9(2)		$7/2^+$	$\rightarrow$	$3/2^+$	$E2$	2
251.7			$[11/2^+]$	$\rightarrow$	$[9/2^+]$	$M1/E2$ [d]	11
252.4	1.01(2)	[b]	$15/2^-$	$\rightarrow$	$11/2^-$	$E2$	1
261.7	0.52(5)		$25/2^+$	$\rightarrow$	$23/2^+$	$M1/E2$	9
263.7	0.45(3)		$27/2^+$	$\rightarrow$	$25/2^+$	$M1/E2$	8
272.0			$29/2^+$	$\rightarrow$			
277.8			$[13/2^+]$	$\rightarrow$	$[11/2^+]$	$M1/E2$ [d]	10
295.6				$\rightarrow$	$25/2^+$		
312.2			$[15/2^+]$	$\rightarrow$	$[13/2^+]$	$M1/E2$ [d]	11
312.8			$13/2^+$	$\rightarrow$	$11/2^+$	$M1/E2$ [d]	3
321.3	0.35(3)		$29/2^+$	$\rightarrow$	$27/2^+$	$M1/E2$	9
332.7			$[17/2^+]$	$\rightarrow$	$[15/2^+]$	$M1/E2$ [d]	10
340.3			$23/2^+$	$\rightarrow$	$21/2^+$	$M1/E2$ [d]	8
346.4	0.33(3)		$31/2^+$	$\rightarrow$	$29/2^+$	$M1/E2$	8
352.4	1.0(3)	0.2(2)	$9/2^+$	$\rightarrow$	$5/2^+$	$E2$	3
360.0	3.0(15)		$[9/2^+]$	$\rightarrow$	$7/2^+$	$M1/E2$	10
372.9	0.50(14)		$23/2^+$	$\rightarrow$	$21/2^-$	$E1$	4
376.8			$[19/2^+]$	$\rightarrow$	$[17/2^+]$	$M1/E2$ [d]	11
386.8	0.33(5)		$33/2^+$	$\rightarrow$	$31/2^+$	$M1/E2$	9
403.4	1.0(1)	0.31(4)	$11/2^+$	$\rightarrow$	$7/2^+$	$E2$	2
405.7			$27/2^+$	$\rightarrow$	$25/2^+$	$M1/E2$ [d]	8
420.0	0.37(16)		$25/2^+$	$\rightarrow$	$23/2^+$	$M1/E2$	5
426.7	0.9(2)		$17/2^-$	$\rightarrow$	$[13/2^-]$	$E2$ [d]	6
432.6	0.55(9)		17/2	$\rightarrow$	$19/2^-$	$\lvert\Delta I\rvert=1$	
434.1	0.25(9)		$29/2^+$	$\rightarrow$	$27/2^+$	$M1/E2$	5
443.3	1.01(9)	>0.2 [c]	$23/2^+$	$\rightarrow$	$19/2^+$	$E2$	4
458.4	1.01(2)	[b]	$19/2^-$	$\rightarrow$	$15/2^-$	$E2$	1
500.1	1.02(9)	0.4(1)	$19/2^+$	$\rightarrow$	$15/2^+$	$E2$	4
519.0							7
525.0							
525.2			$27/2^+$	$\rightarrow$	$23/2^+$	$E2$ [d]	8
529.1			$[13/2^+]$	$\rightarrow$	$[9/2^+]$	$E2$ [d]	10
534.5							7
540.3	1.1(2)	>0 [c]	$13/2^+$	$\rightarrow$	$9/2^+$	$E2$	3
548.7	1.10(7)	0.4(2)	$15/2^+$	$\rightarrow$	$11/2^+$	$E2$	2
558.2			$19/2^+$	$\rightarrow$	17/2		
561.5	1.1(2)		$21/2^-$	$\rightarrow$	$17/2^-$	$E2$	6
563.1	1.0(2)		$23/2^+$	$\rightarrow$	$19/2^+$	$E2$	8
568.0			$29/2^+$	$\rightarrow$	$25/2^+$	$E2$ [d]	9
576.7	1.0(1)	>0.3 [c]	$27/2^+$	$\rightarrow$	$23/2^+$	$E2$	4
583.0							
585.0			$29/2^+$	$\rightarrow$	$25/2^+$	$E2$ [d]	9
589.2	1.0(3)		$[27/2^+]$	$\rightarrow$	$[23/2^+]$	$E2$ [d]	2
589.9			$[15/2^+]$	$\rightarrow$	$[11/2^+]$	$E2$ [d]	11
590.1	0.92(7)		$29/2^+$	$\rightarrow$	$25/2^+$	$E2$	5
601.0			$27/2^+$	$\rightarrow$	$27/2^-$	$E1$ [d]	4
616.7	0.76(6)			$\rightarrow$	$21/2^-$	$M1/E2$	7
630.9	0.96(2)	[b]	$23/2^-$	$\rightarrow$	$19/2^-$	$E2$	1

TABLE I. (*Continued*.)

Energy [a] [keV]	DCO ratio	Polarization	I_i^π	→	I_f^π	Multipolarity	Band
644.7			$[17/2^+]$	→	$[13/2^+]$	$E2$ [d]	10
649.7	0.9(3)		$[23/2^+]$	→	$19/2^+$	$E2$ [d]	2
653.2	0.9(2)					$E2$	7
662.9	1.2(3)		$[17/2^+]$	→	$13/2^+$	$E2$	3
667.7			$31/2^+$	→	$27/2^+$	$E2$ [d]	8
680.8	1.1(1)	>0 [c]	$19/2^+$	→	$15/2^+$	$E2$	2
683.0				→	$[17/2^+]$		3
701.8	0.95(5)	0.3(3)	$31/2^+$	→	$27/2^+$	$E2$	4
726.2	0.8(2)		$25/2^-$	→	$21/2^-$	$E2$	6
733.4			$33/2^+$	→	$29/2^+$	$E2$ [d]	9
737.4	0.93(7)		$33/2^+$	→	$29/2^+$	$E2$	5
779.9	0.95(3)	[b]	$27/2^-$	→	$23/2^-$	$E2$	1
781.0							7
790.6			$[29/2^-]$	→	$25/2^-$	$E2$ [d]	6
803.7	1.11(14)	<0 [c]	$23/2^+$	→	$23/2^-$	$E1$	4
813.2	1.0(1)	1.0(2)	$35/2^+$	→	$31/2^+$	$E2$	4
850.0			$21/2^-$	→	$23/2^-$	$M1/E2$ [d]	6
879.3			$[33/2^-]$	→	$[29/2^-]$	$E2$ [d]	6
885.3			$[37/2^+]$	→	$33/2^+$	$E2$ [d]	5
891.2	0.38(8)		17/2	→	$15/2^-$	$\|\Delta I\|=1$	
907.9	1.01(4)	[b]	$31/2^-$	→	$27/2^-$	$E2$	1
915.8			$[39/2^+]$	→	$35/2^+$	$E2$ [d]	4
919.1	0.18(9)	-0.4(3)	$17/2^-$	→	$19/2^-$	$M1/E2$	6
950.8	0.64(18)	-0.2(2)	$[13/2^-]$	→	$15/2^-$	$M1/E2$ [d]	6
991.3	1.13(15)	-0.80(13)	$19/2^+$	→	$19/2^-$	$E1$	4
996.4			$[43/2^+]$	→	$[39/2^+]$	$E2$ [d]	4
998.4	1.0(1)	0.4(3)	$39/2^-$	→	$35/2^-$	$E2$	1
1002.5	1.0(1)	0.2(2)	$35/2^-$	→	$31/2^-$	$E2$	1
1014.4	0.96(7)		$43/2^-$	→	$39/2^-$	$E2$	1
1034.1	0.49(12)	>0 [c]	$29/2^+$	→	$27/2^-$	$E1$	5
1044.0	0.63(15)					$M1/E2$	7
1061.5	0.28(6)		$21/2^-$	→	$19/2^-$	$M1/E2$	
1207.8	0.4(2)	0.3(1)	$29/2^+$	→	$27/2^-$	$E1$	
1213.4	0.5(2)	0.0(2)		→	$31/2^-$	$\|\Delta I\|\leqslant 1$	
1223.4	0.59(5)	0.3(1)	$25/2^+$	→	$23/2^-$	$E1$	5
1339.2	0.7(2)	0.6(3)		→	$27/2^-$	$\|\Delta I\|\leqslant 1$	
1365.1	0.54(11)	0.6(2)	$25/2^+$	→	$23/2^-$	$E1$	9
1377.2	1.8(5)		$17/2^-$	→	$15/2^-$	$M1/E2$	6
1382.8	0.49(7)	0.4(3)	$25/2^+$	→	$23/2^-$	$E1$	
1394.1	0.50(8)	0.3(3)	$21/2^+$	→	$19/2^-$	$E1$	8
1479.9	1.0(2)		$21/2^-$	→	$19/2^-$	$M1/E2$	6
1502.1	0.4(2)					$\|\Delta I\|\leqslant 1$	7
1539.7	0.51(8)	0.5(2)	$21/2^+$	→	$19/2^-$	$E1$	9
1575.8	0.8(3)		$25/2^-$	→	$23/2^-$	$M1/E2$	6
1577.5							7
1578.7							

[a] Uncertainty in transition energy ± 0.2 keV.

[b] Transition used for the $5\times$Ge polarimeter sensitivity calibration.

[c] The exact value of the polarization cannot be determined because of the complex spectrum.

[d] Transition multipolarity not based on R_{DCO} and polarization measurements (see text).

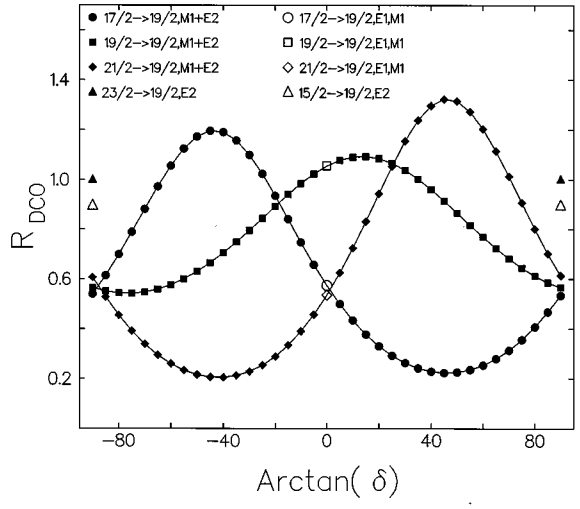

FIG. 3. DCO ratios versus mixing ratio δ calculated for the different spin hypotheses for the 991-keV transition (458-keV gate) in ^{127}La. The spin alignment parameter was set to $\sigma/I=0.3$.

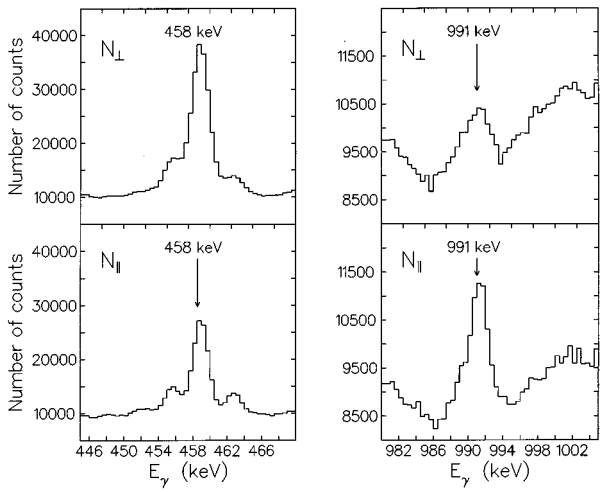

FIG. 5. γ-ray polarization spectra for the 458-keV stretched $E2$ transition and the 991-keV $E1$ $\Delta I=0$ transition in ^{127}La. $N_{\perp}$ labels the spectra with analyzers set perpendicular to the beam axis while $N_{\parallel}$ labels the spectra with analyzers set parallel to the beam axis.

the positive polarization for the 681- keV γ ray, a stretched $E2$ transition is proposed, and stretched $E2$ transitions are suggested for the other cases as well. Spins and parities for band 3 are assigned based on $R_{\rm DCO}$ values measured for the 177- and the 176-keV transitions (which suggest $|\Delta I|\leqslant 1$) and $R_{\rm DCO}$ and polarization values for the 352- and 540-keV transitions (consistent with stretched $E2$ character).

Bands 10 and 11 form a strongly coupled structure. The bands are too weak to extract any experimental information for the transitions, except an $R_{\rm DCO}$ for the 360-keV transition. Based on this value, $9/2^+$ is suggested for the bandhead. A band with similar structure has also been observed recently in ^{131}Pr [18].

The spin/parity assignments of band 6 are based on the $R_{\rm DCO}$ measured for the 919-keV transition. Because $R_{\rm DCO}=0.18(9)$, only a mixed $M1+E2$ assignment with $\Delta I=\pm 1$ is allowed (see Fig. 3). The presence of the 1377-keV transition, which decays from the same excited state as the 919-keV transition, fixes the spin of this state to $17/2^-$. The DCO ratios for the 427-, 562-, and 726-keV transitions are consistent with stretched $E2$ character. Assuming a collective $\Delta I=2$ nature for band 6, $13/2^-$ is proposed for the lowest band member, although this spin assignment is tentative since other possibilities cannot be experimentally excluded. Stretched $E2$ multipolarities are also suggested for the 791- and 879-keV transitions. The spin assignments proposed for band 6 differ from Ref. [9].

A unique determination of the spins of band 7 from the present experiment is impossible. The $R_{\rm DCO}$ of the 617-keV transition suggests mixed $M1+E2$ multipolarities. Based on this information, the parity of band 7 is determined as negative. The only information avaliable for the intraband transitions is an $R_{\rm DCO}$ for the 653-keV transition, which is consistent with a stretched $E2$ assignment. The different spin possibilities for the excited states are shown in the level scheme.

For the 194-, 262-, 264-, 321-, 346-, and 348-keV transitions, which belong to bands 8 and 9, the DCO ratios suggest mixed $M1+E2$ multipolarities with a $|\Delta I|=1$ character. For the other transitions, the statistics were too low to perform the DCO analysis. The level scheme and the presence of connecting $M1+E2$ transitions suggest that bands 8 and 9 form strongly coupled structures. The spin/parity of these bands were determined by the DCO and polarization measured for the 1365- and 1540-keV transitions, which are consistent with a stretched $E1$ character. The assignment is confirmed by the $R_{\rm DCO}$ measured for the 563-keV γ ray, which favors stretched $E2$ transition.

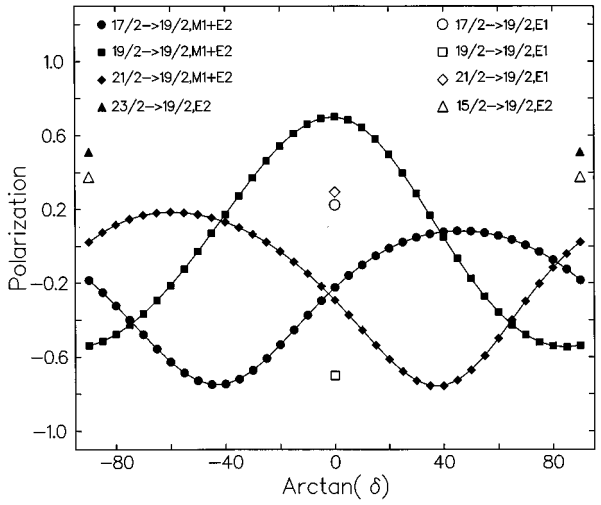

FIG. 4. Polarization versus mixing ratio δ calculated for the different spin and/or parity hypotheses for the 991-keV transition in ^{127}La. The spin alignment parameter was set to $\sigma/I=0.3$.

B. Spin/parity assignments for ^{125}La excited states

Only limited information about high-spin states in ^{125}La was known prior to this experiment. Three transitions assigned to the yrast $h_{11/2}$ band were seen in Ref. [2]. In the present experiment, the yrast cascade was extended by four new transitions and four new collective structures were found. The spins and/or parity assignments for ^{125}La were

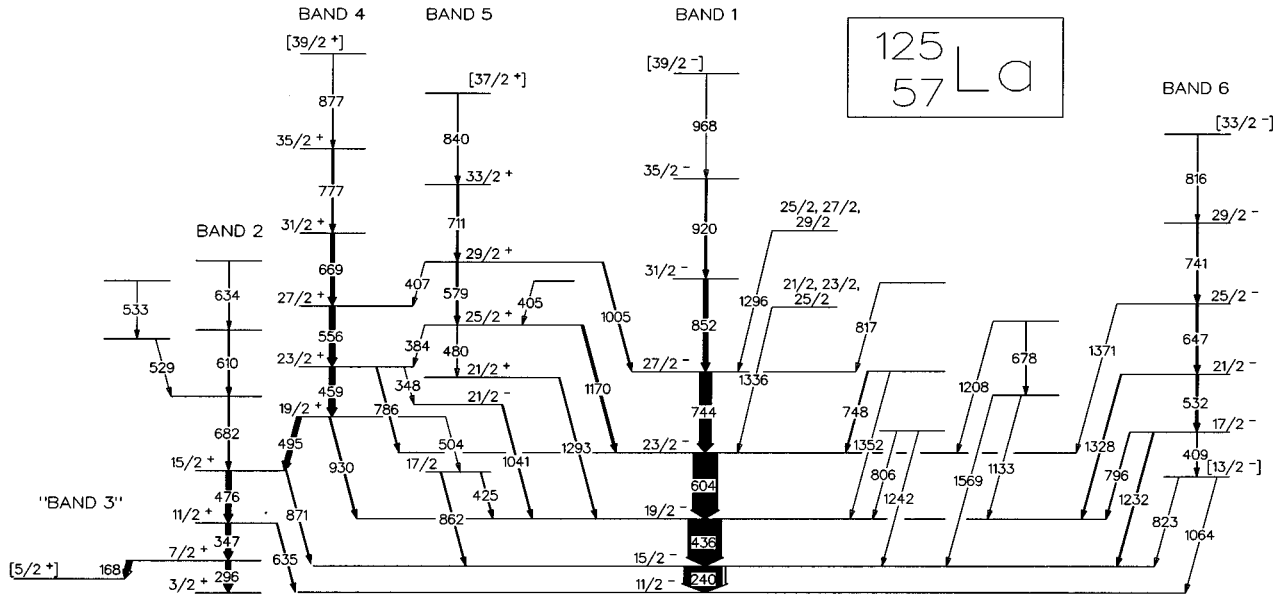

FIG. 6. ^{125}La level scheme.

based mainly on the results of DCO analyses. For band structures similar to those in ^{127}La, systematic arguments were used. The data are summarized in Fig. 6 and Table II.

The DCO ratios extracted for all of the γ rays belonging to band 1 (except 968 keV) are consistent with stretched $E2$ transitions. The DCO ratios for the 1296- and 1336-keV transitions side-feeding band 1 suggest $|\Delta I| \leqslant 1$ and are consistent with stretched $E1$ or mixed $M1+E2$ multipolarities; therefore, the parity of these two levels cannot be determined, and only possible spin values are given in Fig. 6.

The similarity between band 4 in the ^{125}La and band 4 in ^{127}La is strong. In ^{125}La, this band decays to band 1 via 930- and 786-keV transitions (which correspond to the 991- and 804-keV transitions in ^{127}La). For both transitions, the R_{DCO} is close to 1, which is consistent with $I \rightarrow I$ $E1$ transitions as in ^{127}La. Band 4 consists of stretched $E2$ transitions which result from DCO ratios measured for the 459-, 556-, 669-, and 777-keV γ rays. The decay paths from band 4 via the 348- and 1041-keV transitions, the 504-, 425-, and 862-keV transitions, and the 930- and 786-keV transitions are again very similar to the decay paths of band 4 in ^{127}La. The DCO ratios for the 348- and 1041-keV transitions are consistent with stretched dipoles, which together with the similarity to ^{127}La, suggest $21/2^-$ for the intermediary level.

Band 5 is similar to band 5 in ^{127}La; it decays mainly to the yrast band via the 1005-, 1170-, and 1293-keV transitions. Except for the 1170-keV transition, the DCO ratios are consistent with pure stretched dipoles. The decay path to band 4 is via the 384- and 407-keV transitions. The R_{DCO} for the 384-keV γ ray excludes multipolarities other than $M1+E2$ with $|\Delta I|=1$. The DCO ratios for the intraband transitions are in agreement with a stretched $E2$ assignment, if a two standard-deviation limit is allowed for the 579- and 711-keV transitions. Based on these arguments as well as on the similarity to ^{127}La, it is proposed that band 5 consists of stretched $E2$ transitions with the lowest band member assigned $21/2^+$.

Band 4 decays to band 2 via a strong 495-keV transition. The R_{DCO} for this transition is consistent with a stretched $E2$. Polarization and DCO measurements for the corresponding transition in ^{127}La support this assignment. The DCO ratios for the 476-, 347-, and 296-keV γ rays suggest stretched $E2$ transitions. If each of these four transitions (296, 347, 476, 495 keV) are stretched $E2$, then the spin/parity of the bandhead is $3/2^+$ in agreement with the odd-even La systematics (see the discussion concerning the corresponding band in ^{127}La). The consequence of such an assignment is that the 635- and 871-keV transitions have a $I \rightarrow I$, $E1$ multipolarity; the DCO ratios measured for these γ rays are in good agreement with these assignments. The $7/2^+$ level of band 2 decays via the 168 keV transition to a level which corresponds to the $5/2^+$ member of band 3 in ^{127}La. Thus a $5/2^+$ assignment is proposed for this level.

The 796-, 1232-, and 1328-keV γ rays depopulating band 6 have DCO ratios which are consistent with $|\Delta I| \leqslant 1$ and mixed $M1+E2$ multipolarities. The 532-, 647-, and 741-keV γ rays have R_{DCO} values consistent with stretched $E2$ transitions. These data suggest negative parity and a decoupled structure for band 6, as proposed for the corresponding band in ^{127}La. Branching ratios for ^{125}La, ^{127}La are presented in Tables III and IV.

IV. DISCUSSION OF ROTATIONAL STRUCTURES

A. Pairing-deformation self-consistent TRS model

The experimentally observed rotational structures in ^{125,127}La are discussed using the recently developed pairing-deformation self-consistent total Routhian surface (SC-TRS) model [19,20]. The underlying idea of the TRS model is based on the shell correction method of Strutinsky [21]. Within this model, the total Routhian of the nucleus (energy in the rotating frame) is calculated as a sum of a macroscopic part (employing the liquid drop model of Ref. [22]) and a

TABLE II. Observed γ-ray transitions and spin and/or parity assignments for excited states in ^{125}La.

Energy [a] [keV]	DCO ratio	I_i^π	$\rightarrow$	I_f^π	Multipolarity	Band
167.6	0.91(7)	$7/2^+$	$\rightarrow$	$[5/2^+]$	$M1/E2$	2
240.4	1.03(2)	$15/2^-$	$\rightarrow$	$11/2^-$	$E2$	1
296.4	1.01(7)	$7/2^+$	$\rightarrow$	$3/2^+$	$E2$	2
347.4	0.98(5)	$11/2^+$	$\rightarrow$	$7/2^+$	$E2$	2
347.6	0.50(8)	$23/2^+$	$\rightarrow$	$21/2^-$	$E1$	4
384.2	0.20(14)	$25/2^+$	$\rightarrow$	$23/2^+$	$M1/E2$	5
404.9	0.56(10)		$\rightarrow$	$25/2^+$	$\lvert\Delta I\rvert\leqslant 1$	
406.7		$29/2^+$	$\rightarrow$	$27/2^+$	$M1/E2$ [b]	5
408.7	1.1(1)	$17/2^-$	$\rightarrow$	$[13/2^-]$	$E2$	6
425.4	0.36(4)	17/2	$\rightarrow$	$19/2^-$	$\lvert\Delta I\rvert=1$	
436.4	0.98(2)	$19/2^-$	$\rightarrow$	$15/2^-$	$E2$	1
459.2	1.02(6)	$23/2^+$	$\rightarrow$	$19/2^+$	$E2$	4
476.4	1.00(5)	$15/2^+$	$\rightarrow$	$11/2^+$	$E2$	2
480.4	1.05(16)	$25/2^+$	$\rightarrow$	$21/2^+$	$E2$	5
495.3	0.98(5)	$19/2^+$	$\rightarrow$	$15/2^+$	$E2$	4
504.2	0.50(8)	$19/2^+$	$\rightarrow$	17/2	$\lvert\Delta I\rvert=1$	4
529.2	1.0(3)					
532.3	1.03(10)	$21/2^-$	$\rightarrow$	$17/2^-$	$E2$	6
533.0	1.6(6)					
556.4	0.97(8)	$27/2^+$	$\rightarrow$	$23/2^+$	$E2$	4
579.3	0.8(1)	$29/2^+$	$\rightarrow$	$25/2^+$	$E2$	5
603.6	0.98(5)	$23/2^-$	$\rightarrow$	$19/2^-$	$E2$	1
610.3	1.1(1)					2
634.2						2
635.3	1.0(1)	$11/2^+$	$\rightarrow$	$11/2^-$	$E1$	2
646.8	0.97(6)	$25/2^-$	$\rightarrow$	$21/2^-$	$E2$	6
669.3	1.00(8)	$31/2^+$	$\rightarrow$	$27/2^+$	$E2$	4
678.4						
681.5	1.37(16)		$\rightarrow$	$15/2^+$		2
711.0	0.8(1)	$33/2^+$	$\rightarrow$	$29/2^+$	$E2$	5
740.9	0.95(17)	$29/2^-$	$\rightarrow$	$25/2^-$	$E2$	6
744.2	1.03(8)	$27/2^-$	$\rightarrow$	$23/2^-$	$E2$	1
747.7						
777.3	1.01(9)	$35/2^+$	$\rightarrow$	$31/2^+$	$E2$	4
785.8	1.01(12)	$23/2^+$	$\rightarrow$	$23/2^-$	$E1$	4
795.9	0.42(10)	$17/2^-$	$\rightarrow$	$19/2^-$	$M1/E2$	6
806.2			$\rightarrow$	$19/2^-$		
815.7		$[33/2^-]$	$\rightarrow$	$29/2^-$	$E2$ [b]	6
817.4			$\rightarrow$	$27/2^-$		
823.4		$[13/2^-]$	$\rightarrow$	$15/2^-$	$M1/E2$ [b]	6
840.1		$[37/2^+]$	$\rightarrow$	$33/2^+$	$E2$ [b]	5
851.8	0.94(4)	$31/2^-$	$\rightarrow$	$27/2^-$	$E2$	1
862.2	0.10(3)	17/2	$\rightarrow$	$15/2^-$	$\lvert\Delta I\rvert=1$	
871.0	1.04(19)	$15/2^+$	$\rightarrow$	$15/2^-$	$E1$	2
876.8		$[39/2^+]$	$\rightarrow$	$35/2^+$	$E2$ [b]	4
919.6	0.99(5)	$35/2^-$	$\rightarrow$	$31/2^-$	$E2$	1
930.1	1.12(13)	$19/2^+$	$\rightarrow$	$19/2^-$	$E1$	4
968.3		$[39/2^-]$	$\rightarrow$	$35/2^-$	$E2$ [b]	1
1005.3	0.50(4)	$29/2^+$	$\rightarrow$	$27/2^-$	$E1$	5
1041.5	0.47(3)	$21/2^-$	$\rightarrow$	$19/2^-$	$M1/E2$	
1064.4		$[13/2^-]$	$\rightarrow$	$11/2^-$	$M1/E2$ [b]	6
1132.6			$\rightarrow$	$19/2^-$		
1169.9	0.33(2)	$25/2^+$	$\rightarrow$	$23/2^-$	$E1$	5
1208.0			$\rightarrow$	$23/2^-$		
1232.2	0.75(10)	$17/2^-$	$\rightarrow$	$15/2^-$	$M1/E2$	6

TABLE II. (*Continued.*)

Energy[a] [keV]	DCO ratio	I_i^π	→	I_f^π	Multipolarity	Band
1242.0			→	$15/2^-$		
1292.9	0.53(7)	$21/2^+$	→	$19/2^-$	$E1$	5
1296.0	0.40(17)		→	$27/2^-$	$\lvert\Delta I\rvert\leqslant 1$	
1327.9	0.82(9)	$21/2^-$	→	$19/2^-$	$M1/E2$	6
1336.0	0.47(8)		→	$23/2^-$	$\lvert\Delta I\rvert\leqslant 1$	
1352.0			→	$19/2^-$		
1371.0		$25/2^-$	→	$23/2^-$	$M1/E2$ [b]	6
1568.8	0.30(17)		→	$15/2^-$		

[a]Uncertainties in transition energy ± 0.2 keV.

[b]Transition multipolarity not based on DCO analysis (see text).

microscopic correction accounting for shell effects and pair correlations. The total Routhian can be written as

$$E^\omega(Z,N,\hat{\beta}) = E^{\omega=0}(Z,N,\hat{\beta}) + \{\hat{H}^\omega(Z,N,\hat{\beta}) - \hat{H}^{\omega=0}(Z,N,\hat{\beta})\}, \quad (4)$$

where $E^{\omega=0}(Z,N,\hat{\beta})$ represents the liquid drop energy, the single particle shell correction, and pairing energy at frequency zero. The term in the bracket of Eq. (4) describes the change in energy due to rotation. The total Routhian is calculated on a grid in deformation space, including quadrupole (β_2), triaxiality (γ), and hexadecapole (β_4) degrees of freedom, and then minimized with respect to the shape parameters to obtain equilibrium deformations.

In the standard version of TRS, self-consistency is thus related only to the shape degrees of freedom while pairing correlations are treated approximately. The model used here extends the self-consistency requirement to the particle-particle channel. To avoid the well known problems of a sharp superfluid-to-normal phase transition and to make the calculations feasible in a wide frequency range, correlations going beyond the independent quasiparticle scheme (IQ) must be added. Therefore, we restore approximately the particle number symmetry using the ideas of Lipkin, Nogami, and co-workers (LNC) [23], that recently have been extended to the cranking model [24,25,19].

It has been known since the early work of Migdal [26] that the time-odd components of the nuclear mean field and pairing field are of crucial importance for the moments of inertia. The lowest order Migdal term due to the pairing field emerges from quadrupole pairing. The importance of this term has already been discussed by several authors [27–30]. However, in the case of models based on the deformed mean field, special care has to be taken to avoid the spurious shape dependence of quadrupole pairing. To satisfy this requirement we use here the quadrupole pairing interaction defined by ''double-stretched'' generators (see Ref. [20] for details).

Our model Hamiltonian is based on the deformed Woods-Saxon potential [31] employing seniority and quadrupole pairing as a two-body interaction. Two different parametrizations of the Woods-Saxon potential are used. These potentials are denoted as WS-C for the parametrization of Chepurnov [32] and WS-U for the so-called universal parametrization of [33]. A comparative study of the results for the two parametrizations allows us to draw certain conclusions concerning the quality of the single-particle spectrum. The strength of the seniority pairing is calculated using the average gap method of Ref. [34], while the strength of the quadrupole pairing interaction is calculated self-consistently according to the method proposed in Ref. [35]. The model is thus free from adjustable parameters.

The LNC method, being an approximation to the particle number projection, is a step beyond the independent quasiparticle scheme. The formulation of this method, however, allows one to find approximate solutions in the odd-A systems by using formally the language of independent quasiparticle excitations. Hence one can form quasiparticle excitations on top of the LNC solutions that are constrained to $\langle\hat{N}\rangle = odd\ \ number$ (see Ref. [36]). This is of particular importance when studying the problem of diabacity of nuclear motion. Indeed, it appears extremely difficult to calculate self-consistent diabatic energy surfaces for blocked configurations while construction of such surfaces for approximate solutions seems to be considerably easier. In the era of new detector arrays allowing for complete spectroscopy, the necessity of having a good diabatic model is unquestioned. Therefore, one of the issues that will be addressed here is the quality of approximate solutions.

In the following sections, the discussion will be focussed on ^{127}La, since the the structure of ^{125}La is very similar. The differences between the two La isotopes will be addressed later.

B. Negative-parity bands

Three negative parity bands were identified in the present experiment in ^{127}La. Similar structures, populated to higher spin, were observed by the Chalk River group [9]. This high-spin work will also be included in the theoretical comparisons.

For band 1, the $I^\pi = 11/2^-$ bandhead is assigned to be the proton $[550]1/2^-$ deformed Nilsson state originating from the spherical $\pi h_{11/2}$ intruder subshell. Rotational bands involving the $h_{11/2}$ proton orbital are commonly observed in the $A\sim 120$–130 mass region. The aligned angular momentum is almost constant at $i\approx 5\hbar$, implying that the motion of the odd proton can be regarded as decoupled from the even-even core. An upbend that is associated with the alignment of a pair of $h_{11/2}$ neutrons occurs at $\hbar\omega\approx 0.5$ MeV. In the same frequency region, band 1 is crossed by band 4.

TABLE III. Branching ratios for the ^{127}La excited states.

I_i	$E_{\gamma 1}$ [keV]	$E_{\gamma 2}$ [keV]	$I_{\gamma 1}/I_{\gamma 2}$	Band	I_i	$E_{\gamma 1}$ [keV]	$E_{\gamma 2}$ [keV]	$I_{\gamma 1}/I_{\gamma 2}$	Band
$7/2^+$	176.6	236.0	6.3(6)	2	$25/2^-$	1575.8	726.2	1.0(2)	6
$11/2^+$	227.6	403.4	0.17(1)	2		1577.5	534.5	1.7(4)	7
$13/2^+$	312.8	540.3	0.12(3)	3		519.0	616.7	0.41(4)	7
17/2	432.6	891.2	0.54(7)		$23/2^+$	194.2	340.3	1.5(2)	8
$19/2^+$	991.3	500.1	1.99(6)	4	$23/2^+$	563.1	340.3	1.1(2)	8
$19/2^+$	558.2	500.1	0.49(2)	4	$27/2^+$	263.7	525.2	4.0(4)	8
$23/2^+$	803.7	443.3	0.41(2)	4	$27/2^+$	405.7	525.2	0.63(8)	8
$23/2^+$	372.9	443.3	0.10(1)	4	$31/2^+$	346.4	667.7	2.1(3)	8
$27/2^+$	601.0	576.7	0.10(1)	4	$25/2^+$	212.0	261.7	0.79(6)	9
$25/2^+$	420.0	1223.4	0.21(3)	5	$25/2^+$	1365.1	261.7	0.71(8)	9
$29/2^+$	434.1	590.1	0.22(3)	5	$29/2^+$	321.3	585.0	3.9(5)	9
$29/2^+$	1034.1	590.1	0.61(7)	5	$29/2^+$	568.0	585.0	0.9(2)	9
$17/2^-$	919.1	426.7	0.97(13)	6	$29/2^+$	272.0	585.0	0.8(2)	9
$17/2^-$	1377.2	426.7	1.18(14)	6	$[13/2^+]$	277.6	529.1	1.8(2)	10
$21/2^-$	850.0	561.5	0.20(6)	6	$[17/2^+]$	332.7	644.7	2.0(8)	10
$21/2^-$	1479.9	561.5	0.55(12)	6	$[15/2^+]$	312.2	589.9	1.6(3)	11

Figure 7 shows the results of our theoretical calculations (small symbols) for the lowest one-quasiproton ($\pi=-,\alpha=\mp 1/2$) configurations, where π,α denote parity and signature quantum numbers, respectively. In the language of the cranked shell model, the lowest configurations of ($\pi=-,\alpha=\mp 1/2$) are often labeled $E(F)$, respectively. The left panel presents the calculated total Routhian, e^{ω}, versus rotational frequency while the right panel shows the angular momentum, $\langle I_x \rangle$, as a function of $\hbar\omega$. The figure shows the results of both self-consistent and non-self-consistent calculations (see the figure caption for further details).

The absolute energy scale of the calculations is not determined but the excitation energy is relevant. The agreement between the data (band 1) and results of the self-consistent calculations (E) is remarkably good (see Fig. 7). Note that the relative difference between experimental and theoretical Routhians is of the order of 200 keV over the whole frequency range considered. The crossing frequency seems to be slightly underestimated while the yrast-yrare interaction is somewhat too large when compared to the data. The calculations predict a prolate shape of the nucleus with $\beta_2 \approx 0.26$ (predictions for the WS-C potential) until the $\nu h_{11/2}$ alignment. The ^{126}Ba ''core'' is extremely γ soft. The occupation of the $h_{11/2}$ orbital by the odd proton makes the prolate minimum deeper, but the shape remains still rather soft in the low-frequency region, as shown in the TRS plot of Fig. 8. The aligning neutrons drive the nucleus towards a less elongated and slightly triaxial shape ($\beta_2 \approx 0.22, \gamma \approx -5°$ at $\hbar\omega = 0.60$ MeV). The resulting deformation versus frequency trajectories are very similar for both WS-C and WS-U potentials.

The non-self-consistent solutions also offer a reliable approximation to the data. Nevertheless, the relative difference between theoretical and experimental Routhians increases with frequency. The sudden drop of the non-self-consistent value of e^{ω} seen at $\hbar\omega \approx 0.3$ MeV is directly related to the alignment of a pair of $h_{11/2}$ protons taking place at that frequency for an *odd-Z core*. The non-self-consistent treatment of the blocked quasiparticle used here does not allow one to fully remove the effect of the changing pairing gap Δ and Fermi level λ. On the other hand, the calculated angular momentum follows rather closely the experimental findings over the whole frequency region.

In the analysis of the excited negative-parity bands, certain problems occur. Within the limit of the independent quasiparticle model, the low-lying negative parity bands must involve an orbital originating from the $\pi h_{11/2}$ subshell. Therefore, the lowest band of negative parity and signature $\alpha = +1/2$ is expected to be built upon the unfavored signa-

TABLE IV. Branching ratios for the ^{125}La excited states.

I_i	$E_{\gamma 1}$ [keV]	$E_{\gamma 2}$ [keV]	$I_{\gamma 1}/I_{\gamma 2}$	Band	I_i	$E_{\gamma 1}$ [keV]	$E_{\gamma 2}$ [keV]	$I_{\gamma 1}/I_{\gamma 2}$	Band
$7/2^+$	167.6	296.4	0.66(3)	2	$25/2^+$	480.4	1169.9	0.33(5)	5
$11/2^+$	635.3	347.4	0.20(4)	2	$29/2^+$	406.7	579.3	0.28(10)	5
$15/2^+$	871.0	476.4	0.10(1)	2	$29/2^+$	1005.3	579.3	0.72(9)	5
17/2	425.5	862.2	0.7(2)		$[13/2^-]$	823.4	1064.4	0.6(2)	6
$19/2^+$	930.1	495.3	0.22(1)	4	$17/2^-$	795.9	408.7	0.40(7)	6
$19/2^+$	504.2	495.3	0.08(1)	4	$17/2^-$	1232.2	408.7	1.33(13)	6
$23/2^+$	785.8	459.2	0.11(1)	4	$21/2^-$	1327.9	532.3	0.40(6)	6
$25/2^+$	384.2	480.4	0.24(6)	5	$25/2^-$	1371.0	646.8	0.14(4)	6

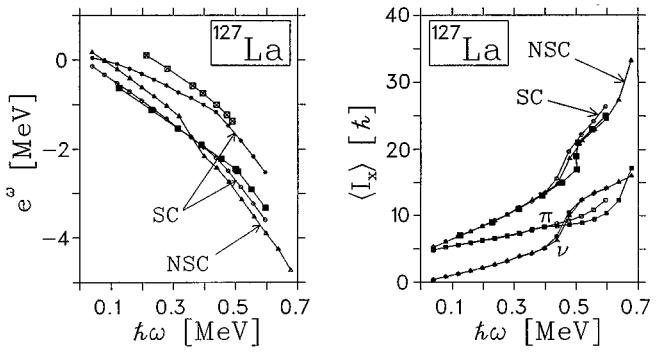

FIG. 7. Theoretical and experimental Routhians (left panel) and angular momentum $\langle I_x \rangle$ (right panel) versus $\hbar\omega$ for negative parity bands in ^{127}La. Experimental data for band 1 (band 6) are denoted by filled (crossed) squares. The results of self-consistent (SC) calculations for the lowest $E(F)$ configuration are denoted by open circles (stars), respectively. The non-self-consistent curves correspond to configuration E. The calculations have been done using the WS-C potential.

ture of the $\pi[550]1/2^-$ orbital. The theoretical prediction concerning this band is shown in Fig. 7. The calculated and experimental bands do not match, independent of spin assignment.

The good agreement between experiment and theory for band 1, as well as for different positive parity bands (see next subsection), suggests that the structure of the negative-parity sidebands involves degrees of freedom beyond our model. In the case of ^{126}Ba, the low-lying vibrational (quasivibrational) states have been observed [37]. It is hence possible that the excited negative-parity side bands are built upon the γ phonon coupled to $\pi h_{11/2}$ as seen in other odd-A isotopes, especially since our calculations predict quite a pronounced softness at low frequencies (see Fig. 8). To further pursue this question, detailed calculations of a particle-vibration coupling type are needed.

C. Positive-parity bands

A simple inspection of the single-particle levels of the Woods-Saxon potential suggests that several positive-parity Nilsson states are accessible for the odd proton depending on deformation. These are the $[420]1/2^+$ and $[422]3/2^+$ Nilsson states forming the pseudo-spin doublet $\widetilde{[321]}$, the $[411]3/2^+$, and $[404]9/2^+$ states. Figure 9 shows quasiproton Routhians calculated at a fixed, moderate deformation of $\beta_2 = 0.25$. At zero frequency the one-quasiproton states form a quadruplet of states with an energy splitting of the order of only 200 keV. At this particular deformation the lowest one-quasiproton excitations involve, in order of energy, $[422]3/2^+$,$[420]1/2^+$,$[411]3/2^+$, and $[404]9/2^+$ states, respectively. However, if a change of deformation or the readjustment of the single particle spectrum of the Woods-Saxon potential is made, the order of these excitations can be easily changed. In fact, at small deformation the $[411]3/2^+$ state is pushed down in energy, while for larger deformation, the $[404]9/2^+$ state comes closest to the Fermi level. Moreover, deformed states originating from the $d_{5/2}$ and $g_{7/2}$ shells are strongly mixed through the deformed mean-field and Coriolis force. Consequently, the structure of the positive-parity bands (especially bands 2 and 3) at low excitation energies cannot be explained unambiguously. This issue will be discussed further.

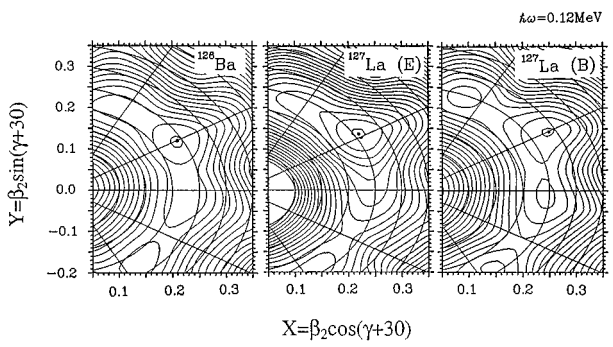

FIG. 8. Total Routhian surfaces calculated at frequency $\hbar\omega = 0.12$ MeV for ^{126}Ba and ^{127}La (configuration E and configuration B). The distance between contour lines corresponds to 200 keV.

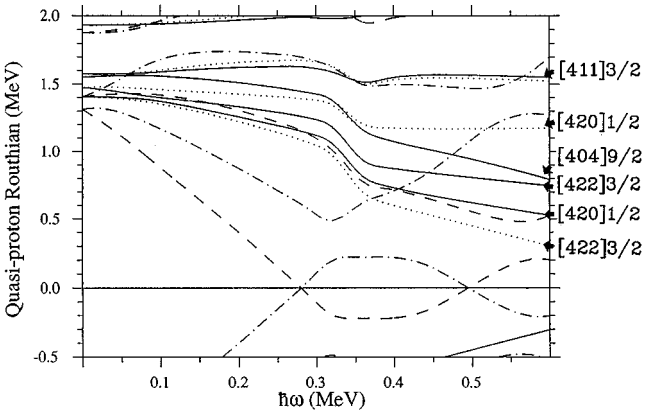

FIG. 9. Proton quasiparticle Routhians as a function of rotational frequency calculated at a constant, moderate deformation $\beta_2 = 0.25$. The following line pattern for different parity-signature (π, α) combinations has been used: solid (dotted) line for $(+,\pm)$; dash-dotted (dashed) lines for $(-,\pm)$, respectively. The positive parity Routhians are denoted by asymptotic Nilsson quantum numbers of the dominant component in the wave function calculated at $\hbar\omega = 0.6$ MeV. The quasiparticle excitations are constructed on top of the $\langle Z \rangle = 57$ vacuum. The drop of the quasiparticle Routhians at $\hbar\omega \approx 0.3$ MeV is caused by $\pi h_{11/2}$ alignment being unblocked in this formalism (see text for details).

Bands 10 and 11

Several of the positive-parity states can be characterized rather uniquely by their distinct features. The $[404]9/2^+$ state leads to a pair of strongly coupled bands, starting with $I = K = 9/2$, with no signature splitting and dominated by $\Delta I = 1$ dipole transitions. According to our model, the $[404]9/2^+$ state should come down in energy at large deformations. The only candidates for this structure are bands 10 and 11 in ^{127}La. Such bands were not observed in ^{125}La. This suggests that the neutron shell structure favors somewhat larger deformation for $N = 70$ than for $N = 68$. In contrast, the WS-C calculations show a pronounced $N = 68$ deformed shell gap. Consequently, the $\pi g_{9/2}$ band calculated by

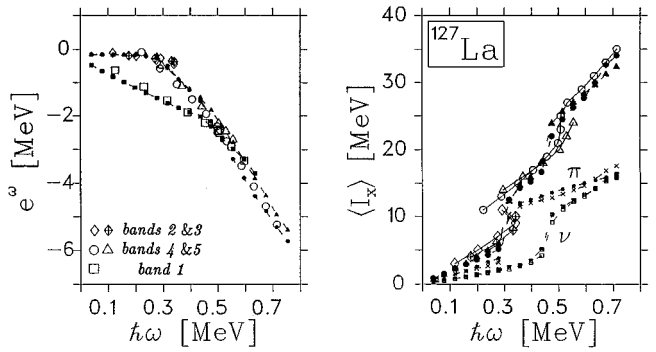

FIG. 10. Theoretical and experimental Routhians (left panel) and angular momentum $\langle I_x \rangle$ (right panel) versus $\hbar\omega$ for positive parity bands in ^{127}La. The Routhian of the negative parity band 1, which is yrast over a wide frequency range, is shown for comparison. Filled symbols represent theoretical points, with squares for the lowest $E(\pi=-,\alpha=-\frac{1}{2})$, triangles for the $A(\pi=+,\alpha=+\frac{1}{2})$, and circles for the $B(\pi=+,\alpha=-\frac{1}{2})$ configurations. The calculations have been done using the WS-U potential.

use of this potential is lowest in energy for both ^{125}La and ^{127}La, contrary to experimental findings. The experimental data seem to be better reproduced by the WS-U potential. In this case the less deformed minima are favored and the $[404]9/2^+$ band is pushed up in energy.

Moreover, due to the combination of the $N=68$ gap of the WS-C potential and the well deformed $Z=58$ gap (the single-particle proton spectra of both WS-C and WS-U potentials are very similar), well-deformed negative-parity structures appear too low in energy both in ^{125}La and ^{127}La. For example, in ^{127}La a well-deformed negative-parity band of signature $\alpha=-1/2$ is predicted to be yrast above $\hbar\omega\sim0.45$ MeV [most probably, it is crossed by the lowest $(\pi=+,\alpha=-1/2)$ band at very high frequencies, but our calculations stop at $\hbar\omega=0.60$ MeV]. Obviously, such a scenario is not supported by the experimental data. For the WS-U potential, a well-deformed band is calculated to become yrast first at the highest observed frequencies. In conclusion, the present set of data do not support the presence of a deformed $N=68$ gap, suggesting that the single-particle spectrum of the WS-U potential is more realistic. One has to bear in mind, however, that due to the very large radius parameters, the use of the WS-U potential requires further renormalization of the Strutinsky moment of inertia (see, e.g., Ref. [38] for details). Unfortunately, such a renormalization is not unambiguous especially in the presence of strong pairing correlations.

Bands 4 and 5

At higher angular momentum, the band built on the favored signature $(\alpha=-1/2)$ of the $[422]3/2^+$ state $(g_{7/2})$ is calculated to be lowest in energy. The signature partner of this band is calculated to be higher than the band built on the favored signature $(\alpha=+1/2)$ of the $[420]1/2^+$ state $(d_{5/2})$ (see Fig. 10). Both features are weakly dependent on deformation. Consequently, at high spins, bands 4 and 5 are interpreted as $\pi[422]3/2^+\otimes\pi(EF)$ and $\pi[420]1/2^+\otimes\pi(EF)$, respectively (see also the discussion in Ref. [39]). One should stress that the $[422]3/2^+$ and $[420]1/2^+$ Nilsson states form a pseudo-spin multiplet $\widetilde{[321]}$ and therefore are strongly mixed. Closer examination of the wave function shows that the $[420]1/2^+$ component of band 5 is dominant over a very wide frequency region. For band 4, our calculations predict a substantial mixing of the $[422]3/2^+$ and the $[420]1/2^+$ states and, at very high frequencies, also with the $[431]1/2^+$ $(g_{7/2})$ state.

The decay pattern of bands 4 and 5 seems to support this scenario. Note that band 5 decays to band 1 via $E1$ transitions and to band 4 through mixed $M1/E2$ transitions. An enhancement of $E1$ transitions is a direct signature of strong octupole mixing between these bands [40]. Indeed, the $\langle[420]1/2^+|r^3Y_{30}|[550]1/2^-\rangle$ matrix element is allowed by the asymptotic quantum numbers and therefore one can expect enhanced $E1$ transitions between bands 1 and 5. As mentioned above, band 4 is calculated to contain a substantial admixture of $[420]1/2^+$. Therefore both $M1/E2$ transitions between bands 4 and 5 as well as $E1$ transitions between bands 4 and 1 are allowed.

Bands 2 and 3

The interpretations of bands 2 and 3 in ^{127}La and band 3 in ^{125}La reveal some interesting features. In ^{127}La, band 4 decays to band 3 by a very weak $E2$ transition, while in ^{125}La the analogous transition is much stronger. Moreover, the I_x vs $\hbar\omega$ curve in ^{125}La shows a curvature characteristic of a low frequency shape change, while in ^{127}La the rotation seems to be regular. The decay pattern thus indicates different microscopic structure for bands 2-3 and 4-5. In terms of the simple single-particle picture, the lowest positive-parity bands at small/moderate deformation involve the $[411]3/2^+$ Nilsson state. Here, the proton $h_{11/2}$ orbits are empty. Due to the strong Coriolis coupling of the high-j orbitals, the proton $h_{11/2}$ orbital is approaching the Fermi surface rapidly. One thus expects the $[411]3/2^+$ "particle" state to be crossed at rather low frequency by $[422]3/2^+$-$[420]1/2^+$ "hole" states, coupled to the aligned $h_{11/2}$ protons. In the presence of pairing correlations, both the occupation of the $h_{11/2}$ orbital and the classification in terms of particle/hole excitations are not very sharp, but the underlying physics might still be valid. This scenario accounts for the weak decay of bands 4 and 5 into bands 2 and 3 as well as the unexpectedly low crossing frequency [37]. In the case of ^{125}La, it implies that the nucleus undergoes a very early shape change leading to strong admixture of $[411]3/2^+$ and $[422]3/2^+$ states. Since we do not calculate each state diabatically, this scenario in our calculations cannot be confirmed.

Bands 8 and 9

Experimentally, there is another pair of strongly coupled bands connected via strong $M1$ transitions, namely bands 8 and 9. No connecting transitions to bands 10 and 11 are observed. The decay goes mainly into bands 1 and 2. In order to calculate microscopically bands 10 and 11, it is necessary to block excited quasiparticles. This is impossible in the present version of our model. Therefore, we give only a qualitative explanation and assignment based on signature splitting arguments extracted from calculated quasiparticle Routhians (see Fig. 9). It is clearly visible from the figure that the only proton orbital having strongly coupled bands

(beyond $[404]9/2^+$) is the $[411]3/2^+$ orbital. One should note that, according to the calculations, the small signature splitting for the $[411]3/2^+$ orbital at low frequencies disappears after the $\pi h_{11/2}$ alignment. This observation is only weakly dependent on deformation. In contrast, the excitation energy of the $[411]3/2^+$ band is strongly deformation dependent. The [411]3/2 orbital becomes more favored at smaller deformation. In the simple particle-hole picture, bands 8 and 9 differ from bands 2 and 3 in terms of a two-particle, two-hole excitation into the $h_{11/2}$ subshell, which might explain the weak decay into band 2.

V. SUMMARY

The properties of the ^{125}La and ^{127}La nuclei have been investigated using the methods of in-beam γ-ray spectroscopy. In addition to the standard γ-γ coincidences and DCO analyses, linear polarizations of γ rays were measured for unique spin and/or parity assignments. A number of collective bands were identified in the experiments.

The observed structures were analyzed using a pairing-deformation self-consistent total Routhian surface model. A detailed discussion of collective structures is given in the text, where the concentration is on the generic features of our model. First, the overall excitation energy scheme is rather well reproduced (aside from the negative-parity sidebands). Nevertheless, at low frequencies the underlying Nilsson configurations could not be uniquely assigned. This could be attributed to the quasiparticle-vibration coupling and/or to the quality of the single-particle spectrum of our Woods-Saxon potential. In fact the calculations indicate quite pronounced γ softness both for positive- as well as negative-parity bands suggesting that the coupling to vibrational degrees of freedom can indeed be of importance. The influence of the single-particle spectrum on the results of our calculations is best visualized for the $[404]9/2^+$ band which was calculated to be yrast for the version involving the WS-C potential, in disagreement with experimental data. Also the $[411]3/2^+$ Nilsson orbital seems to be placed too high in energy, causing certain problems in the interpretation of bands 2 and 3.

At high rotational frequencies, the model works remarkably well. The positive-parity bands 4 and 5 are uniquely interpreted as involving the favored signatures of $\pi[422]3/2^+\otimes(EF)$ and $\pi[420]1/2^+\otimes(EF)$ configurations. Interestingly, $[422]3/2^+$ and $[420]1/2^+$ Nilsson orbitals emerge from the pseudo-spin multiplet $\widetilde{[321]}$ that at least qualitatively, seem to support the decay pattern of band 5. The $\pi h_{11/2}$ band is also well reproduced both concerning the Routhian as well as the angular momentum versus rotational frequency. Note also that the non-self-consistent calculations performed for this band offer a relatively good approximation to the data. Such calculations give much better agreement for the angular momentum than for the Routhian, which shows an artificial drop due to the ''unblocked'' alignment of a pair of $h_{11/2}$ protons.

The negative-parity sideband (including ambiguities in spin assignment) cannot be explained as a one-quasiparticle band built on the unfavored signature of the $\pi h_{11/2}$ orbital. Again, the disagreement seems to have its source in the vibrational degrees of freedom which are beyond our model. This problem, as well as the analysis of low-spin positive-parity bands and electromagnetic properties, will be further investigated in our forthcoming article where the results of the core-quasiparticle model calculations will be presented.

ACKNOWLEDGMENTS

This work was supported in part by the National Science Foundation (U.S.), the UK EPSRC, and the Polish State Committee for Scientific Research (KBN) under Contract No. PB1090/P3/94/06 and No. 2 P03B 034 08. K.H. acknowledges receipt of financial support from the University of York, W.S. financial support from Göran Gustafssons Stiftelse, and R. W. financial support by the Swedish Natural Science Research Council (NFR). The authors would like to thank D.C. Radford for providing the RADWARE software package which was used in data analysis.

[1] S.G. Rohozinski, J. Srebrny, and K. Horbaczewska, Z. Phys. **268**, 401 (1974).
[2] J.R. Leigh, K. Nakai, K.H. Maier, F. Pühlhofer, F.S. Stephens, and R.M. Diamond, Nucl. Phys. **A213**, 1 (1973).
[3] J. Meyer-ter-Vehn, Nucl. Phys. **A249**, 111 (1975); **A249**, 141 (1975).
[4] Y.S. Chen, S. Frauendorf, and G.A. Leander, Phys. Rev. C **28**, 2437 (1983).
[5] P.J. Smith, D.J. Unwin, A. Kirwan, D.J.G. Love, A.H. Nelson, P.J. Nolan, D.M. Todd, and P.J. Twin, J. Phys. G **11**, 1271 (1985).
[6] K. Starosta *et al.* (unpublished).
[7] Ch. Droste, T. Morek, S.G. Rohoziński, D. Albert, H. Grawe, and D. Chlebowska, J. Phys. G **18**, 1763 (1992).
[8] K. Starosta, Ch. Droste, T. Morek, J. Srebrny, D.B. Fossan, D.R. LaFosse, H.S. Schnare, P. Vaska, M.P. Waring, I.M. Hibbert, R. Wadsworth, K. Hauschild, C.W. Beausang, S.A. Forbes, P.J. Nolan, and E.S. Paul, Nuclear Physics Division, Annual Report, Warsaw, 1993, pp. 30 and 32.
[9] D. Ward, V.P. Janzen, H.R. Andrews, S.M. Mullins, D.C. Radford, and J.C. Waddington, in *Proceedings of the International Conference on Nuclear Physics in Our Times, Sanibel, Florida, 1992*, edited by A. V. Ramayya (World Scientific, Singapore, 1993), p. 218; D. Ward, V.P. Janzen, H.R. Andrews, S.M. Mullins, D.C. Radford, and J.C. Waddington, Report No. TASCC-P-93-3.
[10] P.J. Twin, Nucl. Phys. **A409**, 343 (1983).
[11] A. Kramer-Flecken, T. Morek, R.M. Lieder, W. Gast, G. Hebbinghaus, H.M. Jeger, and W. Urban, Nucl. Instrum. Methods A **275**, 333 (1989).
[12] J. Kasagi, N. Kishida, and H. Onhuma, Nucl. Instrum. Methods **144**, 201 (1977).
[13] P.J. Twin, in *The Electromagnetic Interaction in Nuclear Spectroscopy*, edited by W.D. Hamilton (North-Holland, Amsterdam, 1975), p. 716.
[14] P.A. Butler, P.E. Carr, L.I. Gadeken, A.N. James, P.J. Nolan,

J.F. Sharpey-Schafer, P.J. Twin, and D.A. Viggars, Nucl. Instrum. Methods **108**, 497 (1973).
[15] L. Hildingsson, C.W. Beausang, D.B. Fossan, R. Ma, E.S. Paul, W.F. Piel, Jr., and N. Xu, Phys. Rev. C **28**, 2437 (1983).
[16] Y. He, M.J. Godfrey, I. Jenkins, A.J. Kirwan, S.M. Mullins, P.J. Nolan, E.S. Paul, and R. Wadsworth, J. Phys. G **18**, 99 (1992).
[17] R. Wyss, F. Lidén, J. Nyberg, A. Johnson, D.J.G. Love, A.H. Nelson, D.W. Banes, J. Simpson, A. Kirwan, and R. Bengtsson, Nucl. Phys. **A503**, 244 (1989).
[18] Galindo-Uribarri, D. Ward, T. Drake, G. Hackman, V.P. Janzen, S.M. Mullins, S. Pilotte, D.C. Radford, I. Ragnarsson, N.C. Schmeing, and J.C. Waddington, Phys. Rev. C **50**, R2655 (1994).
[19] W. Satuła, R. Wyss, and P. Magierski, Nucl. Phys. **A578**, 45 (1994).
[20] W. Satuła and R. Wyss, Phys. Rev. C **50**, 2888 (1994).
[21] V.M. Strutinsky, Yad. Fiz. **3**, 614 (1966); Nucl. Phys. **A95**, 420 (1967).
[22] S. Cohen, F. Plasil, and W.J. Swiatecki, Ann. Phys. (N.Y.) **82**, 557 (1974).
[23] H.C. Pradhan, Y. Nogami, and J. Law, Nucl. Phys. **A201**, 357 (1973).
[24] P. Magierski, S. Ćwiok, J. Dobaczewski, and W. Nazarewicz, Phys. Rev. C **47**, 2418 (1993).
[25] B. Gall, P. Bonche, J. Dobaczewski, H. Flocard, and P.-H. Heenen, Z. Phys. **A348**, 183 (1994).
[26] A.B. Migdal, Nucl. Phys. **13**, 655 (1959).
[27] S.T. Beliaev, Nucl. Phys. **A24**, 322 (1961).
[28] I. Hamamoto, Nucl. Phys. **A232**, 445 (1974).
[29] M. Wakai and A. Faessler, Nucl. Phys. **A295**, 86 (1978).
[30] M. Diebel, Nucl. Phys. **A419**, 221 (1984).
[31] S. Ćwiok, J. Dudek, W. Nazarewicz, J. Skalski, and T. Werner, Comput. Phys. Commun. **46**, 379 (1987).
[32] V.A. Chepurnov, Yad. Fiz. **6**, 955 (1967).
[33] J. Dudek, Z. Szymański, T. Werner, A. Faessler, and C. Lima, Phys. Rev. C **26**, 1712 (1982).
[34] P. Möller and R. Nix, Nucl. Phys. **A536**, 20 (1992).
[35] H. Sakamoto and T. Kishimoto, Phys. Lett. B **245**, 321 (1990).
[36] P. Ring, R. Beck, and H.J. Mang, Z. Phys. **231**, 10 (1970).
[37] D. Ward, V.P. Janzen, H.R. Andrews, D.C. Radford, G.C. Ball, D. Horn, J.C. Waddington, J.K. Johansson, F. Banville, J. Gascon, S. Monaro, N. Nadon, S. Pilotte, D. Prevost, P. Taras, and R.A. Wyss, Nucl. Phys. **A529**, 315 (1991).
[38] W. Nazarewicz, R. Wyss, and A. Johnsson, Nucl. Phys. **A503**, 285 (1989).
[39] R. Wyss, F. Lidén, J. Nyberg, A. Johnson, D. J. G. Love, A. H. Nelson, D. W. Banes, J. Simpson, A. Kirwan, and R. Bengtsson, Nucl. Phys. **A503**, 244 (1989).
[40] G.B. Hagemann, I. Hamamoto, and W. Satuła, Phys. Rev. C **47**, 2008 (1993).